1 Fundamentals

This chapter gives an introduction of the fundamental aspects of magnetic phenomena, which are relevant to describe the spin-reorientation transition of ultrathin ferromagnetic single and double layers. Since ferromagnetic bilayers have been studied in detail, the direct exchange coupling and the role of local magnetic moments per atom at the interface of two ferromagnetic layers are considered. In order to explain the mechanism of the spin-reorientation transition, the role of magnetic anisotropies and their dependence on both the film thickness and the temperature is discussed. The opposite spin-reorientation transition of ultrathin Ni/Cu(100) and Fe/Cu(100) films and its manipulation by different conditions of the film growth is reviewed. The principles of how magnetic domains and domain walls are formed in ultrathin films being in the thermodynamical ground state and near the spin-reorientation transition is outlined.

1.1 Ferromagnetism in ultrathin 3d bilayer films

The ferromagnetic properties of a solid are correlated with its dimensionality. The spontaneous magnetization, which arises from the parallel alignment of the magnetic moments of atoms due to the exchange interaction is one characteristic observable of a ferromagnet. In contrast to a bulk $3d$ ferromagnet, like Fe, Co or Ni, in which the orbital magnetic moment is almost quenched due to the high symmetry of the arrangement of the surrounding atoms within the crystal, in ultrathin films this quenching is partly lifted due to both the broken symmetry at the surface and the strain as resulting from the epitaxial growth on the substrate [41]. The reduced dimensionality also affects the Curie-temperature, which decreases with decreasing layer thickness of an ultrathin film (finite size effect) [15]. Moreover, thickness and temperature dependent surface and interface magnetocrystalline anisotropies largely contribute to the orientation of the magnetization in ultrathin films [2]. In bilayers, consisting of two different ferromagnetic layers, an additional contribution arises from the interface between the coupled single layers. At this interface the two types of atoms exchange electrons and form the band structure of an alloy. The individual magnetic moments will change, depending on the degree of alloying [42].

1.1.1 Exchange coupling in bilayer systems

In two ultrathin ferromagnetic layers A and B, which are in direct contact, the exchange coupling J^{AB} is strong and orients the magnetic moments of the single layers into a common direction. The exchange energy is based on pair interaction at the interface and yields:

$$E_{ex} \quad = \quad -2J^{AB}\, S^{A} \cdot S^{B} \tag{1.1}$$

where S^{A} and S^{B} are nearest neighbor spins. From the exchange coupling constant J_{AB}, an interface exchange stiffness parameter $A^{AB} = 2J^{AB}S^{A}S^{B}/a^{AB}$ results, where $a^{AB} = \sqrt{a^{A}a^{B}}$, with a^{A} and a^{B} being the lattice spacings of the layers A and B, respectively. A^{AB} can be estimated from the bulk values for Fe and Ni [43]. The total magnetization of the bilayer is the sum $M^{A} + M^{B}$ of the individual magnetizations, whereby the average saturation magnetization is given by $M_S^{av} = (d^{A}M^{A} + d^{B}M^{B})/(d^{A} + d^{B})$ where d^{A} and d^{B} are the thicknesses of the two layers [44]. The ferromagnetic coupling will decrease if the magnetic layers are separated by a non-magnetic interlayer of increasing thickness. An oscillation between a ferromagnetic and an antiferromagnetic coupling as a function of the spacer layer thickness was observed [45].

1.1.2 Magnetic moments at interfaces and in alloys

For the discussion of local magnetic moments at the interface of a ferromagnetic bilayer, like Fe/Ni/Cu(100), it has to be taken into account that even for a perfectly flat Fe/Ni interface there already exists an overlap of the $3d$-bands of the adjacent Fe and Ni layers. For such flat surfaces the coordination number of both the fcc Fe(100) and the fcc Ni(100) layer is reduced from 12 to 8. This reduction is lifted when both surfaces are touching each other. At each atomic site of Fe (Ni), 4 Ni (Fe) atoms supplement the coordination number up to 12. On average, for each interface atom the number of nearest neighbors is 6 Fe atoms and 6 Ni atoms (see Fig. 1.3 (b)). The resulting band structure corresponds to that of an $Fe_{0.5}Ni_{0.5}$ alloy, i. e. Fe and Ni atoms exchange their electrons. The average magnetic moment of the interface may be obtained from the Slater-Pauling curve, which gives the magnetic moment of an alloy as a function of the number of valence electrons per atom (e/a).

The Slater-Pauling curve

The Slater-Pauling curve describes that the average magnetic moment of an Fe_xNi_{1-x} alloy increases with increasing Fe concentration starting from $x = 0$. Due to the fact that variations of the magnetic moment depend only on the relative number of occupied or unoccupied states in the spin-up and spin-down d-bands, and not on the shape of the density of states $Z(E)$ or the state density at the Fermi-level E_F [46], the basic understanding of the Slater-Pauling curve is

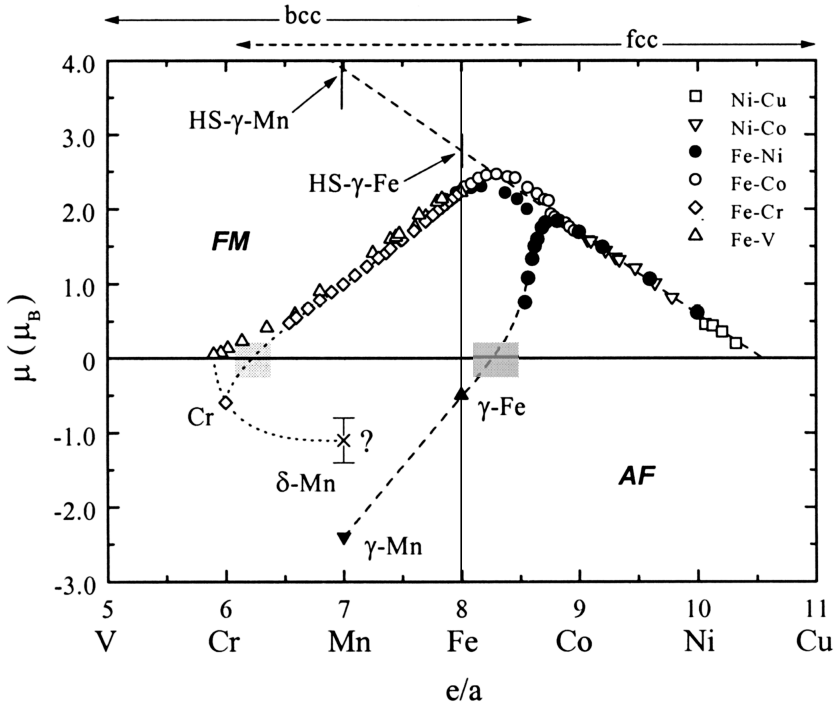

Figure 1.1: The Slater-Pauling curve for an Fe_xNi_{1-x} alloy (•) shows the average magnetic moment ($\mu > 0$) versus the number of valence electrons per atom (e/a). Extrapolation to the ferromagnetic high-spin state of γ-Fe yields $\mu_{\mathrm{Fe}} \approx 2.7\ \mu_{\mathrm{B}}$. The sharp decline around $8.5\ e/a$ is due to a fcc-bcc-phase transformation. The antiferromagnetic ground state ($\mu < 0$) of γ-Fe is indicated by the symbol ▲. (From [47]).

usually given within the rigid-band-model, which assumes that the s- and d-bands are rigid in shape as the atomic number changes.

The spin magnetic moment[1] μ_S per atom of a transition metal alloy is given by the spin imbalance of particularly the d-electrons:

$$\mu_S \approx (n_d^{\uparrow} - n_d^{\downarrow})\,\mu_{\mathrm{B}} \tag{1.2}$$

where $n_d^{\uparrow}$ and $n_d^{\downarrow}$ are the d-subband populations. Generally both $n_d^{\uparrow}$ and $n_d^{\downarrow}$ may vary upon alloying. Starting at $x = 0$, i. e. with pure fcc Ni, one finds the well known magnetic moment of 0.6 μ_{B}. Since Ni is a strong ferromagnet, for which E_F lies above the top of the spin-up (majority) band, the magnetic moment per atom can be simply calculated as:

$$\mu_S = (5 - n_d^{\downarrow})\,\mu_{\mathrm{B}}\ . \tag{1.3}$$

Because $n_d^{\downarrow} = n_d - 5$ and $n_d = n_d^{\uparrow} + n_d^{\downarrow}$ it follows that:

$$\mu_S = (10 - n_d)\,\mu_{\mathrm{B}}\ . \tag{1.4}$$

[1]Only the spin moment is considered; the small orbital contribution to the total magnetic moment is not included in this model.

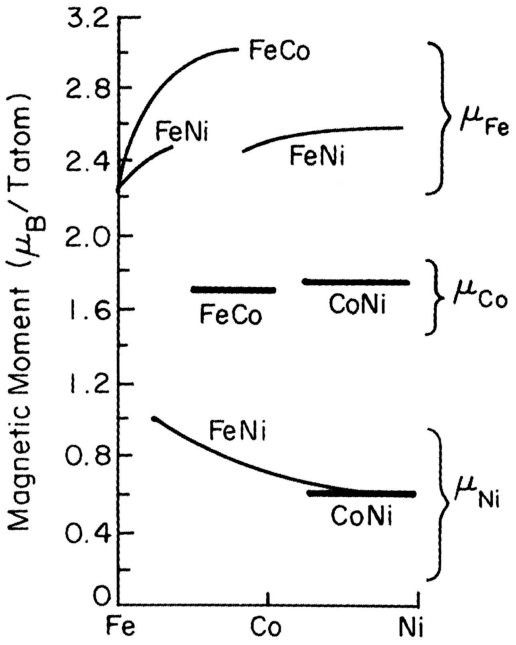

Figure 1.2: Local magnetic moments on Fe and Ni sites for an Fe-Ni alloy determined by neutron scattering measurements. Upon alloying Ni progressively with Fe the magnetic moment of Ni increases while the magnetic moment of Fe declines. (From [46]).

For strong ferromagnets this equation is a straight line with slope -1, meaning a change of $1\ \mu_{\mathrm{B}}$ per valence electron, which is found in the right hand branch of the Slater-Pauling curve in Fig. 1.1. Equation (1.4) also explains, why the average moment of Co should be so close to that of $Fe_{0.5}Ni_{0.5}$, since they both have the same number of valence electrons and thus the same value of n_d. For higher Fe concentrations in fcc Ni, the Fermi-level is continuously lowered, because the number n_d of d-electrons decreases and hence the average magnetic moment increases according to Eq. (1.4). As long as the binary alloy remains in an fcc structure, there is no change in the slope of the Slater-Pauling curve as the Fe concentration is increased. Finally, alloying would end up with pure fcc γ-Fe in the high-spin state. In this state the magnetic moment of γ-Fe, which arises from a large atomic volume, is $\approx$2.7 μ_{B} (see Fig. 1.1).

The average magnetic moment of Fe-Ni alloys with $(e/a) < 8.7$ strongly deviates from the Slater-Pauling curve towards $\mu = 0$ because of a transition to antiferromagnetism in the Fe-rich concentration range. The shaded area in Fig. 1.1 around $\mu = 0$ shows the concentration region where ferromagnetic and antiferromagnetic interactions compete. Such coexisting interactions lead to interesting magnetic states such as spin-glasses [47]. However, before the concentration of the system can reach a composition corresponding to that of a spin-glass state, which occurs at $(e/a) \approx 8.5$, [2] the structure becomes bcc, and the average magnetic moment jumps up to about $2\ \mu_{\mathrm{B}}$. Upon further increase of the Fe concentration, the magnetic moment increases up to the well known bulk value of $2.2\ \mu_{\mathrm{B}}$ for pure bcc α-Fe. The change of the site-resolved magnetic moments per Fe and Ni atom in Fe-Ni alloys determined by neutron scattering measurements

[2] At $(e/a) \approx 8.5$ i. e. for an $Fe_{0.75}Ni_{0.25}$ alloy, the individual magnetic moments have been calculated to be $\mu_{\mathrm{Fe}} = 0.0008\ \mu_{\mathrm{B}}$ and $\mu_{\mathrm{Ni}} = -0.0023\ \mu_{\mathrm{B}}$ [48]

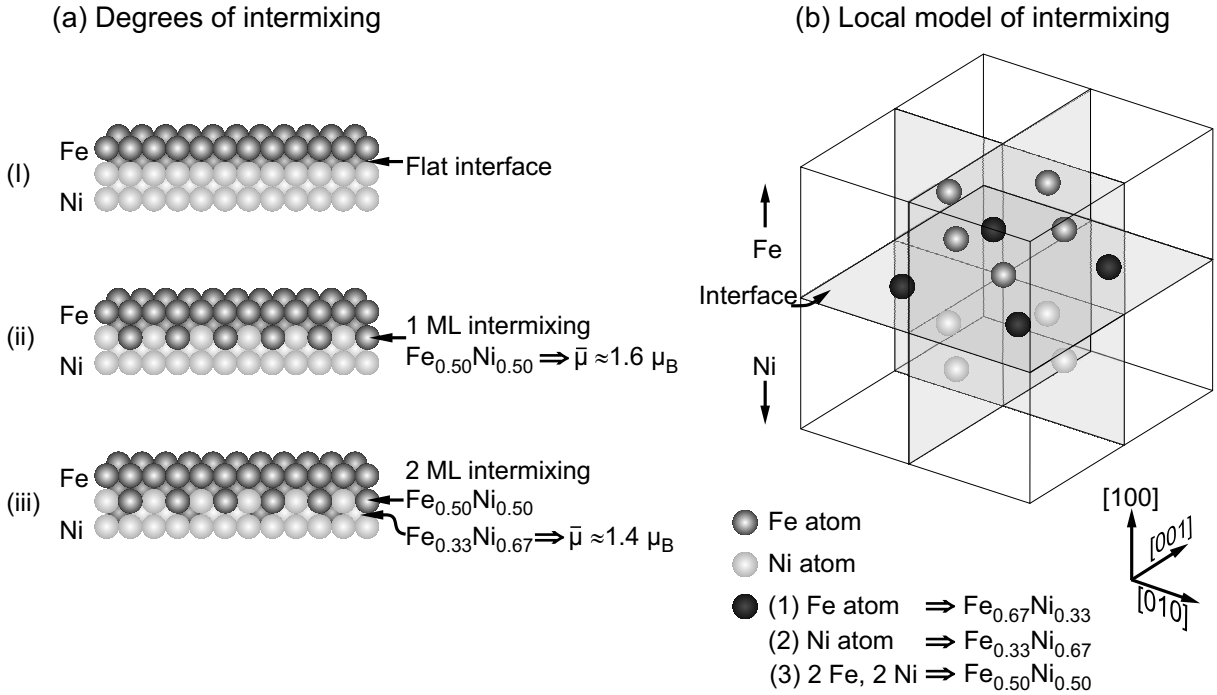

Figure 1.3: The possible degrees of intermixing (a) and the different nearest neighbors at the Fe/Ni interface −assuming fcc growth− of Fe/Ni/Cu(100) (b) give rise to different average magnetic moments according to the Slater-Pauling curve. The centered Fe atom in (b) is located at the interface. Three special cases for the 12 nearest neighbors are sketched by the black spheres: 4 Fe atoms at the interface lead to the Invar-concentration $Fe_{0.67}Ni_{0.33}$ (1), 4 Ni atoms yield an $Fe_{0.33}Ni_{0.67}$ alloy which is near the Permalloy concentration (2) and an equal number of Fe and Ni atoms results in $Fe_{0.50}Ni_{0.50}$ (3).

is presented in Fig. 1.2. It shows that the Ni magnetic moment continuously increases from 0.6 μ_B (bulk value) up to 1.0 μ_B, when the Fe concentration increases, while the moment per Fe atom decreases from $2.6\ \mu_B$ to the bulk value $2.2\ \mu_B$.

At the concentration of $Fe_{0.65}Ni_{0.35}$ the alloy shows the Invar effect [48,49], which is correlated with a nearly vanishing thermal expansion coefficient within a broad temperature interval around 300 K. Fe-Ni alloys in the Invar composition range have a ferromagnetic ground state with a high magnetic moment and a large volume [47]. The underlying principle of this effect is a moment-volume instability [50].

For any deviation from the ideal flat interface due to intermixing of Fe and Ni atoms, the band structure of the interface will be different, leading to a variation in the local magnetic moment of both types of atoms. In Fig. 1.3 three special cases are pointed out, which may result in a strong deviation of local magnetic moments, contributing to an average moment of the bilayer. An intermixing within one monolayer, assuming an equal number of Fe and Ni atoms, gives rise to an $Fe_{0.50}Ni_{0.50}$ alloy as sketched in Fig. 1.3 (a,ii) with an average magnetic moment of $1.6\ \mu_B$ according to the Slater-Pauling curve. If the alloy ranges over two layers as reported in [51], hypothesizing an Fe concentration gradient towards the Ni film, the second layer may

result in an $Fe_{0.33}Ni_{0.67}$ alloy, which is near the Permalloy concentration. The associated average magnetic moment is about $1.4\ \mu_B$. Fig. 1.3 (b) illustrates the 12 nearest neighbors of an Fe atom at the Fe/Ni interface within a three dimensional fcc lattice. The Fe atom in the center is surrounded by four Fe atoms (gray spheres) of the top layer and four Ni atoms (bright spheres) of the bottom layer. Moreover, there are four atoms (dark spheres) within the interface plane, each of them being either Fe or Ni atoms. Depending on whether these four atoms are Fe or Ni atoms, different local magnetic moments of the centered Fe atom are expected. Three special cases are singled out in the figure, which correspond to local magnetic moments per Fe atom at (1) the Invar concentration, (2) the Permalloy concentration and (3) in an $Fe_{0.50}Ni_{0.50}$ alloy.

1.2 Spin-reorientation transition (SRT)

A *spin-reorientation transition* describes how the direction of the easy axis of the magnetization changes upon variation of e. g. the film thickness or the temperature. The modification of the magnetic anisotropy, which determines the orientation of the magnetization, and corresponding changes of the magnetic domains during an SRT are elucidated in the following.

1.2.1 The role of magnetic anisotropies

The magnetocrystalline anisotropy energy (MAE) is the difference in the free energy density associated with different directions of the magnetization with respect to the crystallographic axes of a crystal. The origin of the MAE is the long range dipole-dipole-interaction and the spin-orbit-interaction. The dipolar interaction gives rise to the shape anisotropy, which for a homogeneously magnetized rotational ellipsoid is given by $K_d = \frac{1}{2}\mu_0(N_x M_x^2 + N_y M_y^2 + N_z M_z^2)$, where $N_x + N_y + N_z = 1$ is the trace of the diagonalized demagnetizing tensor. Ultrathin films of a few atomic layers thickness and a lateral size of some millimeters may be described by an ultrathin disc with infinite lateral size, for which $N_x = N_y = N_\parallel = 0$ and $N_z = N_\perp = 1$. The shape anisotropy is then given by $K_d = \frac{1}{2}\mu_0(N_\perp - N_\parallel)M^2$, and it always favors an in-plane orientation of the magnetization for ultrathin films. The spin-orbit-interaction causes the magnetocrystalline (intrinsic) anisotropy, which may lead to either an in-plane or an out-of-plane direction of the magnetization. In ultrathin films, the orientation of the magnetization is determined by the balance between the intrinsic and the shape anisotropy. This balance changes as a function of both temperature and film thickness. We use the generally accepted sign convention, i. e. a positive anisotropy constant favors a perpendicular easy axis. A spin-reorientation transition from an out-of-plane to an in-plane orientation of the magnetization will occur, when the shape anisotropy dominates over a large positive magnetocrystalline anisotropy. The easy axis of the magnetization is determined from the minimum of the free energy density F, which for an ultrathin film with a uniaxial magnetic anisotropy along the surface normal may

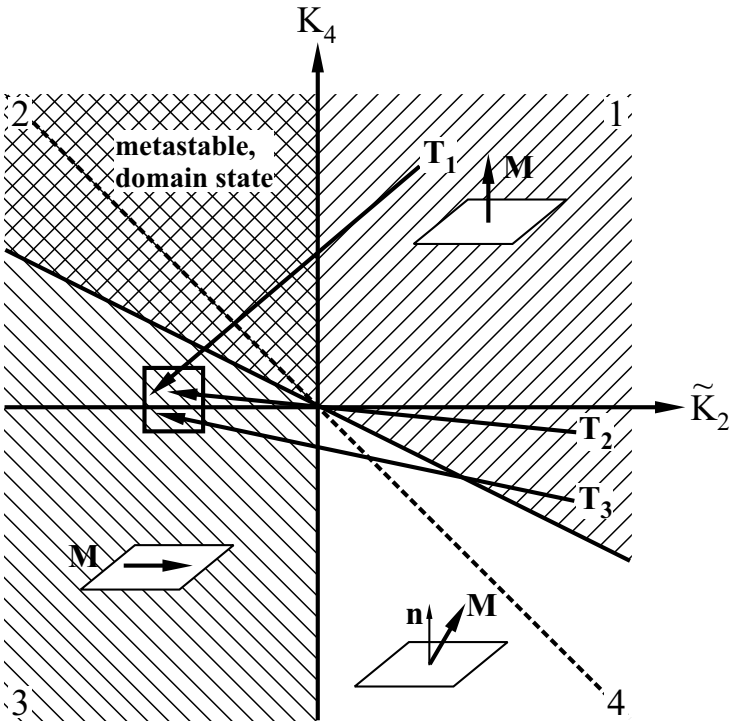

Figure 1.4: Stability diagram of the easy axis of the magnetization without an external magnetic field. Areas of various hatching mean different phases. Three cases of the thickness-driven SRT from out-of-plane to in-plane are illustrated: through the metastable phase (T_1), via the origin (T_2) and through the canted phase (T_3). The dashed line indicates equally deep energy minima. $\tilde{K}_2 = K_2 - \frac{1}{2}\mu_0 M^2$. (After [4,11]).

be written as [11]:

$$F = \left(\frac{1}{2}(N_\perp - N_\parallel)\mu_0 M^2 - K_2\right)\cos^2\theta - K_4\,\cos^4\theta \tag{1.5}$$

where θ is the angle of the magnetization M with respect to the surface normal. The effective magnetocrystalline anisotropy constants K_i are commonly separated into a thickness-independent volume coefficient K^V and a thickness-dependent contribution $2K^S/d$ that includes the surface and interface anisotropy constants [52]:

$$K_i = K_i^V + \frac{2K_i^S}{d} \tag{1.6}$$

with $i = 2, 4$ according to the second- and fourth-order constants, respectively, where d is the film thickness.

A consideration of second-order contributions to the anisotropy only ($K_4 = 0$) does not allow for a canted magnetization vector. Instead, a discontinuous reorientation of the magnetization, which is a first-order SRT, takes place as K_2 changes. The first-order SRT is indicated in Fig. 1.4 [4], [3] which displays K_4 versus $\tilde{K}_2 = K_2 - \frac{1}{2}\mu_0 M^2$, by tracing a trajectory from the perpendicular orientation of the magnetization (first quadrant) to the in-plane oriented magnetization (third quadrant) along the $\tilde{K}_2$-axis ($K_4 = 0$). The critical thickness d_c for the SRT,

[3]The diagram has been modified with respect to the notation used for the free energy density given by Eq. (1.5), i. e. the canted and the metastable phase appear in opposite quadrants as compared to the original work, where the free energy density is given by $F = K_1 \sin^2\theta + K_2 \sin^4\theta + \frac{1}{2}\mu_0 M^2 \cos^2\theta$.

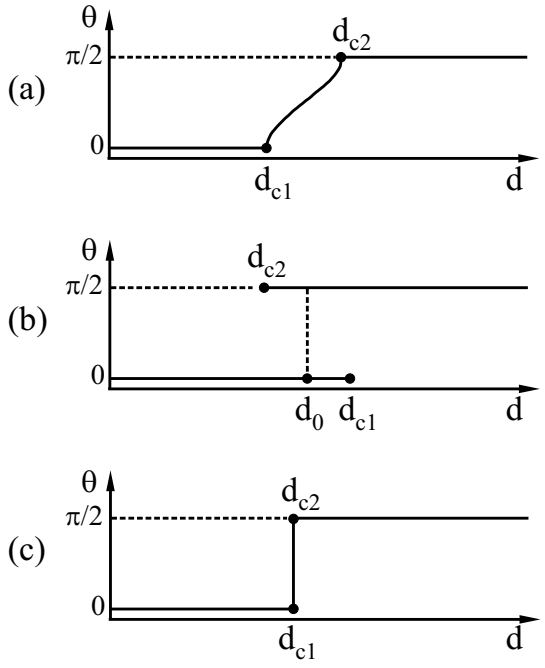

Figure 1.5: Different types of spin-reorientation transitions. The ranges of stability (metastability) are indicated for perpendicular magnetization ($\theta = 0$) and in-plane magnetization ($\theta = \frac{\pi}{2}$). (a) Continuous SRT with a gap between both ranges. (b) Discontinuous SRT with an overlap of the ranges. (c) Special transition. (From [3]).

which arises from the balance $K_2 = \frac{1}{2}\mu_0 M^2$, is given by

$$d_c = \frac{2K_2^S}{\frac{1}{2}\mu_0 M^2 - K_2^V} \tag{1.7}$$

A discontinuous reorientation also occurs if both $\tilde{K}_2$ and K_4 change during the SRT, such that any trajectory T_2 from the in-plane magnetized state to the perpendicularly magnetized state or vice versa passes the origin in Fig. 1.4. The occurrence of a canted magnetization within a continuous SRT is possible, if the fourth-order anisotropy coefficient $K_4 < 0$. In Fig. 1.4, the trajectory T_3, which passes through the fourth quadrant, represents such kind of an SRT. If K_4 becomes positive, the trajectory T_1 passes the hatched area of the second quadrant between in-plane and out-of-plane magnetization states, which describes a metastable configuration of the magnetization. In this case a multi domain state of coexisting out-of-plane and in-plane magnetized domains is possible [11].

In general, if K_4 is non-zero, two critical thicknesses arise, i. e. d_{c1} and d_{c2} corresponding to the onset and the completion of the reorientation process, respectively:

$$d_{c1} = d_c = \frac{2K_2^S}{\frac{1}{2}\mu_0 M^2 - K_2^V} \tag{1.8}$$

$$d_{c2} = \frac{2(K_2^S + 2K_4^S)}{\frac{1}{2}\mu_0 M^2 - (K_2^V + 2K_4^V)} \tag{1.9}$$

Three types of spin-reorientation transitions can be distinguished [3]:

1. *Continuous transition* for $d_{c1} < d_{c2}$, see Fig. 1.5(a). Within an interval $d_{c1} < d < d_{c2}$, both the perpendicularly and the in-plane oriented magnetization represent energetic max-

ima with a minimum in between. The magnetization rotates continuously from $\theta(d_{c1}) = 0$ to $\theta(d_{c2}) = \frac{\pi}{2}$ with increasing d. The anisotropy does not disappear.

2. *Discontinuous transition* for $d_{c1} > d_{c2}$, see Fig. 1.5(b). Within an interval $d_{c2} < d < d_{c1}$, both the perpendicularly and the in-plane oriented magnetization represent energetic minima with a maximum in between. The magnetization switches between both minima at the thickness d_0 (between d_{c2} and d_{c1}), where the depths of both energetic minima become equal. The anisotropy does not totally vanish.

3. *Special transition* for $d_{c1} = d_{c2}$, see Fig. 1.5(c). For this transition the anisotropy vanishes. In a real system this transition can hardly be expected.

For a tetragonally distorted film like e. g. Ni/Cu(100) the anisotropic part of the free energy density is given by [33]:

$$F = \left(\frac{1}{2}\mu_0 M^2 - K_2\right)\cos^2\theta - \frac{1}{2}K_{4\perp}\cos^4\theta - \frac{1}{8}K_{4\parallel}(3+\cos 4\Phi)\sin^4\theta \quad (1.10)$$

where θ is defined as in Eq. (1.5), and Φ is the azimuthal angle measured against the easy in-plane axis of the magnetization. $K_{4\perp}$ and $K_{4\parallel}$ are the fourth-order terms of the MAE, which account for the disparity of the directions perpendicular and parallel to the plane due to the lattice distortion. In consideration of $K_{4\perp}$ and $K_{4\parallel}$ and under the assumption, that the in-plane easy axis of the magnetization does not change during the SRT, i. e. $\Phi = 0°$, the critical thicknesses of the SRT are determined by:

$$d_{c1} = \frac{2(K_2^S - K_{4\parallel}^S)}{\frac{1}{2}\mu_0 M^2 - K_2^V + K_{4\parallel}^V} \quad (1.11)$$

$$d_{c2} = \frac{2(K_2^S + K_{4\perp}^S)}{\frac{1}{2}\mu_0 M^2 - (K_2^V + K_{4\perp}^V)} \quad (1.12)$$

1.2.2 Spin-reorientation transition of Ni/Cu(100) and Fe/Cu(100) films

The spin-reorientation transition of ultrathin Fe/Cu(100) films as a function of temperature and film thickness shows a behavior, which can be regarded as prototypical for ferromagnetic films on most substrates. This thin film system has a large positive surface magnetic anisotropy at low temperatures and thicknesses, which forces the magnetization perpendicular to the film plane. Upon increasing the temperature or Fe layer thickness the magnetization reorients into the plane. Ultrathin Ni/Cu(100) films on the other hand exhibit a reversed SRT from an in-plane direction at low temperatures and thicknesses to a perpendicular orientation of the magnetization at sufficiently high temperatures and layer thicknesses. In the following two subsections the fundamental microscopic phenomena, which on the one hand lead to the SRT in Fe/Cu(100)

and on the other hand to the anomalous SRT in Ni/Cu(100) films are described separately, in detail.

Fe/Cu(100)

In Fe/Cu(100) films the switching of the magnetization from out-of-plane to in-plane, as the Fe thickness or the temperature is increased, is accompanied by structural changes in the ultrathin film, which have a crucial influence on the magnetic properties. Bulk Fe is known to crystallize in the body-centered-cubic (bcc) phase (α-Fe). The face-centered-cubic (fcc) phase (γ-Fe) is thermodynamically unstable at 300 K [53]. It occurs in the temperature range of 1184 K to 1665 K, and no ordered magnetic structure is found in this high-temperature range [54].

When Fe is deposited on Cu(100), however, a ferromagnetic order exists with a perpendicular magnetic anisotropy between 2 ML and $4-5$ ML Fe [55,56]. The lattice mismatch between fcc Cu ($a_{\mathrm{Cu}} = 0.361$ nm) and fcc Fe ($a_{\mathrm{Fe}} = 0.359$ nm) is about 1%. At room temperature (RT), ultrathin Fe films have been observed to exhibit a layer-by-layer growth [57–59]. Below 1.6 ML interdiffusion of Fe and Cu occurs due to the relatively higher surface energy of Fe as compared to Cu(100), such that Fe clusters form, which are embedded in the Cu surface [58]. In the subsequent thickness interval up to $4-5$ ML, Fe films grow in a shear-distorted face-centered-cubic structure as revealed by scanning tunneling microscopy (STM) [60]. It was shown that a few atoms wide bcc-like stripes were formed, which in order to compensate the lattice mismatch lead to a zigzag deformation of the original straight atom rows. The shear angle was found to be $\pm 14^{\circ}$ [60,61]. The ferromagnetism was earlier explained by a large atomic volume ($V = 0.0121$ nm^3) of Fe, which arises from an expansion of both the in-plane and the vertical interlayer distance (tetragonally distorted fcc lattice) [62]. Also the shear-distorted fcc lattice observed by STM is accompanied by an enhancement of the atomic volume, giving rise to the ferromagnetism [60].

Upon increasing the Fe layer thickness, a structural transformation to the fcc phase takes place above 4 ML Fe, which is stable in the range of 5 ML to 10 ML [63]. A good layer-by-layer growth is observed in this thickness range. The Fe layers consist of large islands, having a relaxed fcc structure, and showing a smaller lattice constant of $a = 0.357$ nm ($V = 0.0114$ nm^3). This has been predicted theoretically to be associated with an antiferromagnetic order [64] (see Fig. 1.1.2). Elongated bcc phase inclusions are responsible for the observed relaxation [54,65].

Two ferromagnetic "live layers" ($T_C = 280$ K) with a perpendicular anisotropy have been detected in Fe/Cu(100) films between 5 ML and 10 ML thickness by polar magneto-optical Kerr effect (MOKE) measurements [57]. By utilizing Mössbauer spectroscopy the interior layers are found to be paramagnetic at 300 K, and they are in an antiferromagnetic ground state, exhibiting a low magnetic moment of $\mu_{\mathrm{Fe}} < 0.7\ \mu_{\mathrm{B}}$, below the Néel-temperature $T_N = 65$ K [66,67]. In

contradiction, one ferromagnetic surface layer in the fct structure with a $T_C = 250$ K, and a $T_N = 200$ K for the interior layers in the fcc structure was reported by Li et al. [29]. Two different spin configurations in the interior layers of a 6 ML Fe/Cu(001) film, namely a stable ground state and a metastable state, respectively, have been determined [68]. In the stable state, pairwise ferromagnetically coupled layers were joined, which couple antiferromagnetically to each other, whereas in the metastable state each layer was found to couple antiferromagnetically to the adjacent one. A recent investigation of an 8 ML Fe/Cu(100) film by means of depth-resolved x-ray magnetic circular dichroism (XMCD) confirmed the existence of two ferromagnetically coupled surface layers. Moreover, strong evidence was found that the inner layers were in a spin density wave (SDW) state, where the amplitude of the SDW was comparable to the magnetic moment in the ferromagnetic (FM) Fe layers. Furthermore, the FM/SDW interface coupling was discovered to be antiferromagnetic [69].

As the Fe thickness exceeds 11 ML, a structural transformation from fcc to bcc occurs, and the magnetization rotates into the film plane with the easy axis along the [110] direction of the Cu-crystal, which in turn is aligned parallel to the [100] axis of Fe. In this state the film is homogeneously magnetized, but it exhibits a rough surface, since it is difficult for the bcc Fe phase to adopt the fcc structure of the underlying Cu-substrate [54]. The structural transformation from γ-Fe to α-Fe, and hence the SRT can be retarded in the presence of oxygen to a thickness of up to 45 ML on top of the Cu. The surfactant effect of oxygen gives rise to an improved layer-by-layer growth of γ-Fe due to a Cu(001)-O($2\sqrt{2} \times \sqrt{2}$)R45° reconstruction. A fully developed bcc structure with an in-plane orientation of the magnetization is achieved around 53 ML Fe [70].

In low temperature-(LT)-grown Fe/Cu(100) interdiffusion between Fe and Cu is reduced, and the films are rougher as compared to RT-grown films. Below 0.9 ML a growth of double-layered islands is observed, followed by a layer-by-layer growth up to $4-6$ ML, where the SRT occurs [71]. In LT-grown Fe/Cu(001) films, which have been annealed to 300 K, an extremely high value of $K^V = 1.8 \times 10^6$ J/m^3 was found, which arises from strain as resulting from a 6% vertical expansion of the distorted fcc Fe layers as compared to the fcc phase. This value of K^V is two orders of magnitude larger than that for bcc Fe films. Both K_2^V and $2K_2^S$ represent large perpendicular anisotropy energies, and they determine the perpendicular easy axis of the magnetization of the distorted fcc Fe film. The SRT toward an in-plane direction of the easy axis of the magnetization around 10 ML was attributed to the reduction of K^S with increasing Fe layer thickness, whereas it was not directly attributed to the structural transformation from fcc to bcc as reported generally [72].

The temperature-driven SRT in ultrathin films of $2.5-3.5$ ML is found to be a reversible process [27]. The observation of a temperature dependent SRT is based on the temperature dependence of the anisotropy constants. This leads to the conclusion, that the surface anisotropy

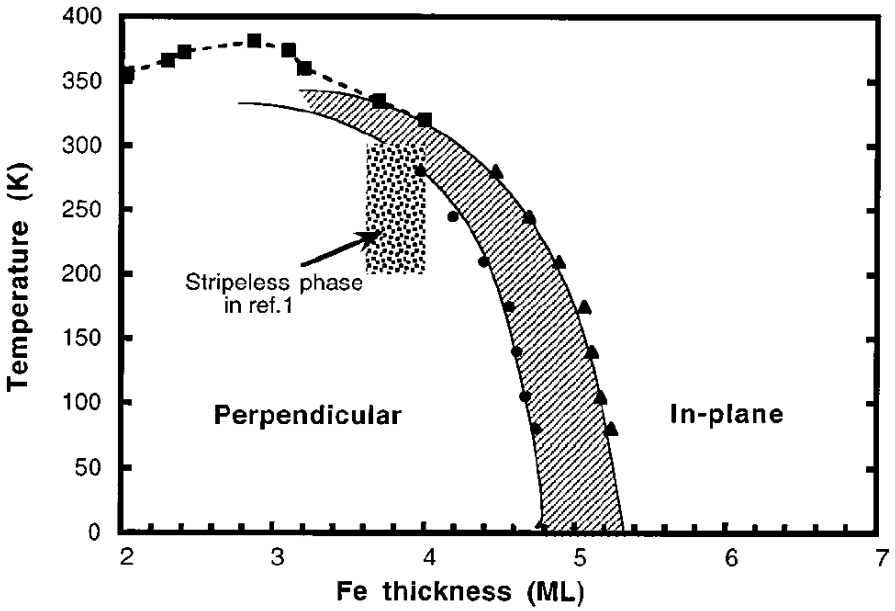

Figure 1.6: Magnetic phase diagram of fct Fe on Cu(100) taken from Ref. [73]. The hatched area is the transition regime in which the magnetization is either canted, or composed of both perpendicular and in-plane magnetic domains. The rectangular shaded area identifies the temperature and thickness regime, in which an fct-to-fcc structural transformation occurs, and where a stripeless phase was found [12].

energy decreases faster than the shape and volume anisotropy energy, when the temperature is increased [74]. Furthermore, the temperature dependence of the magnetocrystalline surface and volume anisotropy constants has been discussed using a spin fluctuation model [75]. The results demonstrate that thermal fluctuations have a much weaker effect on the surface anisotropy as compared to the bulk anisotropy of a cubic material, because for the surface case the next closest energy minimum is 180° away, as opposed to only 90° in the case of the bulk [74].

Across the SRT, the evolution of stripe domains with a preferential orientation along the [001] direction being stable against thermal fluctuations, was theoretically predicted [76]. Such an occurrence of stripe domains was confirmed by spin-polarized scanning electron microscopy [28].

The adsorption of atoms and molecules can affect the SRT decisively. The SRT at 293 K was found to occur under a hydrogen atmosphere of 5×10^{-6} Pa around 6 ML Fe/Cu(001) [77], which is the critical thickness of the magnetization reorientation observed earlier in Fe/Cu(100) films grown and measured at 100 K [78]. Moreover, the fcc phase, which is known to form within the thickness range of about $4 - 10$ ML in RT-grown Fe films, did not occur during the film growth under the hydrogen atmosphere at 293 K. Hence, there is strong evidence, that the known different structural phase transitions and the according magnetic properties between LT- and RT-grown and measured Fe/Cu(100) films are due to the adsorption of hydrogen when the film is cooled during growth. In a recent study it was found, that CO on top of an Fe/Cu(100)

film shifts the critical thickness d_c to smaller Fe thicknesses by at most 0.7 ML. This is explained by a reduction of the surface anisotropy term from $K^S = 0.89$ mJ/m^2 to $K^S = 0.63$ mJ/m^2. Upon oxygen adsorption a complete reorientation of the easy axis into the film plane was observed for all thicknesses down to 2 ML Fe [55].

The coverage of Fe/Cu(100) films with fractions of a Co layer can help to determine the "real" critical thickness $d_c = 3.5$ ML (LT-grown) and $d_c = 4.8$ ML (RT-grown) [31]. Using this method the SRT of Fe is induced by the negative effective anisotropy of the Co coverage, *before* the structural transformation of the Fe film from fct to fcc occurs. The amount of Co, which is necessary for the SRT, decreases linearly with increasing Fe layer thickness. Finally, the extrapolation to an evanescent Co thickness yields the "real" critical thickness of the SRT of Fe/Cu(100). A critical thickness of $d_c = 4.3$ ML (LT-grown) was discovered by using Ni adatoms [79], as if there was no structural phase transition. The reorientation of the easy axis from perpendicular to in-plane results from the in-plane anisotropy of the Fe-Co and Fe-Ni interface, respectively. Using this method with Co-adatoms, Pierce et al. [73] developed the magnetic phase diagram for fct Fe/Cu(100) as depicted in Fig. 1.6. Moreover, it was found that the SRT induced by Co-capping, proceeds via a multi domain formation [80]. By changing the spatial arrangement of the Co atoms on top of the Fe layers as a function of the annealing temperature two opposite SRT directions can be obtained. (i) A temperature of 150 K $<$ T$_{\text{anneal}}$ $<$ 250 K firstly leads to a rotation of the easy axis of the magnetization from out-of-plane to in-plane, and (ii) upon further annealing up to 300 K, the magnetization rotates back into the out-of-plane direction [32].

Investigations of Fe/Cu(100) films by photoelectron spectroscopy revealed that films close to 2 ML Fe thickness have a unique electronic structure, which is not predicted by calculations of bulk fcc Fe, nor do they correspond to bulk bcc Fe. The Fermi-surface exhibits significant changes at the SRT around 4 ML to 5 ML thickness [30].

A reversed SRT from an in-plane to an out-of-plane magnetization orientation, as found for Ni/Cu(100) ultrathin films, is also observed in pulsed-laser-deposited ultrathin Fe/Cu(100) films. Within the thickness range of 2 ML to 5 ML the magnetization lies in the plane, followed by a region where the direction of the magnetization is perpendicular to the surface (6 ML to 10 ML). At a thickness of around 11 ML, the magnetization reorients into the plane again, which is associated with the well known fcc-to-bcc transformation. Observation of this behavior was only possible because of an improved layer-by-layer growth, achieved by the high deposition rate of 1 ML/min [81].

Ni/Cu(100)

The first 15 Ni layers grow pseudomorphically on Cu(100) [82]. Due to the lattice mismatch between fcc Ni ($a_{\text{bulk}} = 0.352$ nm) and fcc Cu ($a_{\text{bulk}} = 0.361$ nm) the Ni layers grow in the

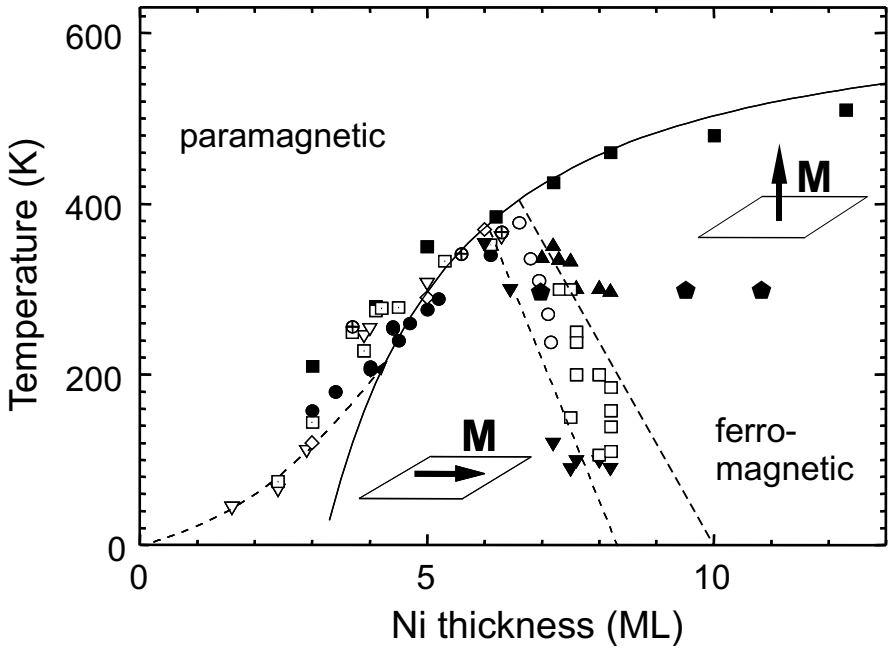

Figure 1.7: Magnetic phase diagram of Ni/Cu(001) as a function of the film thickness d. The solid line indicates the finite size scaling, the straight dashed lines are guides to the eye. Details for the various symbols are given elsewhere [37,84]. The pentagons indicate the SRT thickness at 300 K determined by SPLEEM (this work). In the area between in-plane and out-of-plane orientation of the magnetization solid triangles up (down) indicate out-of-plane (in-plane), open circles and squares mean $0^\circ < \theta < 90^\circ$ orientation of the magnetization. (From [85]).

fct structure on Cu(100). Thereby, the in-plane lattice constant of Ni is expanded by 2.5%, and the vertical interlayer spacing is compressed by 3.2% as compared to the bulk values. This tetragonal distortion is the reason for the large positive volume anisotropy constant $K_2^V = 30\ \mu$eV/atom at 300 K [37], which favors an out-of-plane orientation of the magnetization. The positive sign of K_2^V results from the negative magnetostriction constant of Ni [15,33]. Both the Cu-Ni interface anisotropy constant $K_2^{\text{Cu-Ni}} = -59\ \mu$eV/atom and the Ni surface-to-vacuum anisotropy constant $K_2^{\text{Ni-vac}} = -107\ \mu$eV/atom [83] are negative, and they therefore favor an in-plane orientation of the magnetization. The shape anisotropy $\frac{1}{2}\mu_0 M^2 = 7.5\ \mu$eV/atom [9] also favors an in-plane magnetization direction. The only contribution, which favors a perpendicular magnetization direction arises from the magnetocrystalline volume anisotropy, which is the key to understand the anomalous SRT of Ni/Cu(100). Fig. 1.7 shows the magnetic phase diagram of Ni/Cu(001) as a function of the temperature and the layer thickness. Below 5 ML the film is in the paramagnetic state at 300 K. According to a finite size fit (solid line) it becomes visible, how the Curie-temperature T_C of this system depends on the Ni layer thickness. At 5 ML the Curie-temperature reaches room temperature. Between 5 ML and 7 ML the magnetization is oriented in the plane, which means that in this thickness regime the sum of the shape anisotropy

and the negative surface and interface anisotropy overcomes the positive volume anisotropy contribution. Since the sum of the surface and the interface contribution is thickness dependent, according to Eq. (1.6) their influence decreases upon increasing the thickness.

At an initial critical thickness $d_c = 7-10$ ML [7,37,86,87], the anisotropies, which favor an in-plane and a perpendicular orientation of the magnetization, respectively, are balanced such that this marks the onset of the SRT to an out-of-plane magnetization orientation. This thickness is given by Eq. (1.7), if higher-order anisotropies are ignored. A more detailed consideration, which accounts also for the data points ranging in the thickness interval between the dotted lines in Fig. 1.7, yields two critical thicknesses d_{c1} and d_{c2}, which are given by Eq. (1.11) and (1.12). The data points between the dotted lines in the figure represent canted magnetization configurations, i. e. the magnetization continuously reorients from an in-plane orientation to an orientation perpendicular to the surface with increasing layer thickness.

In a narrow thickness interval around 7 ML the SRT may also be observed as a function of the temperature. The magnetocrystalline anisotropy coefficients K_2 and K_4 were determined by angular dependent FMR measurements [8,85]. The magnetization angle was found to change continuously, indicating a second-order SRT with an upper and a lower critical thickness d_{c1} and d_{c2}, respectively. The SRT is explained by the temperature dependence of the interface and the volume contributions of the anisotropy [88]. The anomalous SRT via a canted magnetization is also confirmed by theoretical calculations [5], which are in good agreement with the experimental data of Ref. [8,85].

There are a number of conditions, which have been proven to influence the SRT of Ni/Cu(100) films. Studies of the influence of the growth temperature on the SRT reveal, that the critical thickness of LT-grown (170 K) films, which have been annealed to 300 K, is about 1 ML smaller than that of an RT-grown film. A higher density of small rectangular islands is observed in the LT-grown film of 8.5 ML thickness as compared to the RT-grown film, whereas the crystalline structure is fct in both cases. By calculating the difference in SRT thicknesses, $d_c^{RT} - d_c^{LT}$, a reduced surface anisotropy in the LT-grown Ni film is found to be the main reason for the smaller critical thickness [89].

Ni films grown on a stepped Cu-surface, for instance, with a (1 1 32) orientation show nearly the same critical thickness of the SRT (5.5 ML to 7 ML) at 300 K as compared to Ni films grown on a flat Cu(100) substrate. However, a canted magnetization with angles of $20^\circ - 30^\circ$ with respect to the surface normal is observed. In addition, a 90° in-plane rotation of the magnetization is observed, resulting in an orientation perpendicular to the step edges [90]. A spiral-like rotation of the magnetization vector from an in-plane orientation parallel to the step edges, to an out-of-plane orientation perpendicular to the steps has been discovered, which is explained by an extra anisotropy originating from steps at the Cu(001) surface [10]. A systematic investigation of the SRT thickness was performed by Bovensiepen *et al.*, who grew

Ni films on curved Cu(001) substrates. These measurements indicated that the SRT thickness is invariant in a range of $0^\circ - 7^\circ$ of the vicinal angle [24]. Calculations ($T = 0$) of a Ni film with a (1 1 13) stepped surface predicted an additional SRT, in which the magnetization turns from parallel to perpendicular to the step alignment with increasing Ni film thickness. This should originate from the presence of a uniaxial magnetoelastic volume anisotropy contribution, caused by tetragonal strain in the film due to film/substrate lattice mismatch, however, at a thickness of about 16 ML [91].

The SRT has also been studied on planar Cu-substrates with different crystallographic orientations such as Cu(100) in comparison to Cu(110) and Cu(111). Qualitatively, the same SRT as compared to Ni/Cu(100) films was reported by Wu *et al.* [92], however, at a much larger reorientation thickness of $d_c = 16$ ML at 300 K. In contradiction to this result, no easy axis of the magnetization perpendicular to the surface was found in Ni/Cu(110) films up to 28 ML thickness in a recent study at 300 K [93]. No perpendicular magnetization is detected in Ni/Cu(111) films down to 3 ML [92].

Capping of an ultrathin Ni/Cu(100) film with a non-magnetic layer like Cu, reduces the critical thickness of the SRT, because the Ni-Cu interface anisotropy $-$although negative$-$ is smaller than that of the Ni surface of the respective uncapped film. 1 nm of Cu reduces the critical thickness by 1 ML [23]. Using a cap of the same element as for the substrate like in Cu/Ni/Cu allows one to differentiate between the interface anisotropy $K_2^{\text{Cu-Ni}}$ and the surface anisotropy $K_2^{\text{Ni-vac}}$, by comparison with the $2K_2^S$ of the uncapped Ni/Cu(100) film[4]. On the other hand, capping ultrathin Ni/Cu(100) with 2 ML of Co increases the magnitude of the surface anisotropy, which forces the magnetization of the Ni film in-plane, at least for thicknesses up to 18 ML [94].

Another procedure, which leads to an SRT from perpendicular to in-plane, has recently been investigated for 6 nm and 9 nm Cu-capped Ni/Cu/Si(001) films without changing the film thickness or temperature. Irradiation of the film with 1 MeV C^+-ions reduced the in-plane strain, such that the magnetization reoriented into the film plane [95].

Growth temperature as well as the exposure of adsorbates can significantly shift the critical thickness d_c of the SRT. A complete hydrogen coverage for example reduces d_c by about 4 ML with respect to a clean Ni surface [9], which in turn is in good agreement with a theoretical analysis [67]. Also adsorption of CO decreases d_c due to a decrease of the surface anisotropy [96]. Besides, an improved layer-by-layer growth after oxygen preadsorption onto the Cu(001) surface is observed, the SRT is shifted from about $10 - 11$ ML (without preoxidation) to about 5 ML Ni thicknesses. Additionally, an in-plane rotation of the magnetization from the [110] to the [100] direction is obtained, when the Ni film is grown on the oxygen-pre-covered Cu(001) [83,97].

[4] $2K_2^S = K_2^{\text{Cu-Ni}} + K_2^{\text{Ni-vac}}$

1.3 Magnetic domains

This chapter addresses the nature of magnetic domains in ultrathin ferromagnetic films. In section 1.3.1 the formation of magnetic domains in the thermodynamic equilibrium as a consequence of the long-range magnetic dipole-dipole interaction is outlined. Typical types of domain walls separating both perpendicularly and in-plane magnetized domains are described in section 1.3.2. An extensive review about various types and the formation of magnetic domains can be found in the textbook of Hubert and Schäfer [17].

1.3.1 The thermodynamic ground state of magnetic domains

In its thermodynamic ground state a ferromagnet usually consists of differently oriented magnetic domains, i. e. regions in which the magnetic moments are aligned parallel. The exchange interaction is responsible for this parallel alignment of magnetic moments, and it is restricted to short-range interaction among adjacent spins. Magnetic domains are formed, in order to reduce the energetically unfavorable magnetic stray field outside of the sample, which originates from the long-range dipole-dipole interaction. However, energy is consumed in order to configure the domain walls, i. e. the transition regions between the domains. Within a domain wall, the magnetization rotates continuously from its direction within one domain into the direction within an adjacent domain. This results in energetically unfavorable orientations of the magnetic moments with respect to the easy axes determined by the magnetic anisotropy. The two simplest types of domain walls are Bloch walls and Néel walls, which are described in section 1.3.2. The total free energy density of a domain configuration is given by the sum of the exchange energy, the magnetocrystalline anisotropy, the dipolar energy, the magneto-elastic energy and the Zeeman energy (if an external magnetic field is applied). By minimizing the total free energy density the most stable domain configuration is then attained.

1.3.2 Domain walls in ultrathin films

The width of a domain wall is determined by the competition between the exchange energy, which is lowest for a large number of magnetic moments including small canting angles between each other, and the anisotropy energy, which favors a low number of magnetic moments oriented off the easy direction of the magnetization. The exchange contribution to the surface energy density σ (J/m^2) of a 180°-domain wall is given by [46]:

$$\sigma_{ex} \approx J\,S^2\,\frac{\pi^2}{N\,a^2} \tag{1.13}$$

where J is the exchange integral, S the spin quantum number, N the number of atomic magnetic moments and a the lattice constant. An increase of N denotes an increased number of magnetic

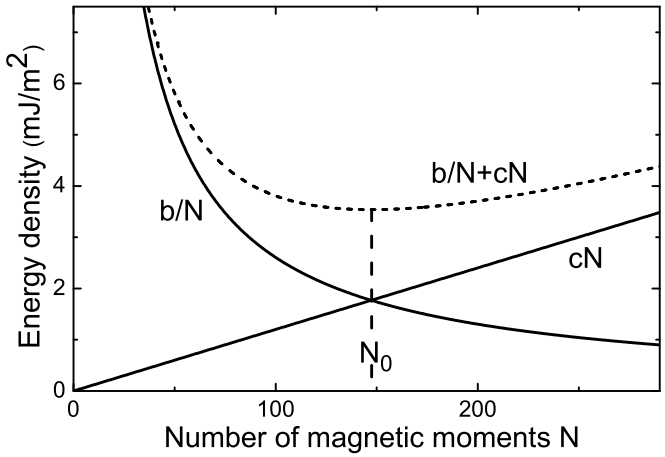

Figure 1.8: Determination of the equilibrium number N_0 of magnetic moments involved in the reorientation transition within a domain wall of a bulk-like Fe/Cu(100) film by minimization of the sum of exchange b/N and anisotropy energy density cN (Eq. (1.15)). The minimum of the sum (dotted curve) occurs for $b/N = c\,N$, i. e. $N_0 = \sqrt{b/c} = 147$ using $J = 2.16 \times 10^{-21}$ J, $K_2^{\text{eff}} = 4.2 \times 10^4$ J/m^3 and $a = 2.86 \times 10^{-10}$ m.

moments oriented in directions of higher anisotropy energy density according to:

$$\sigma_{an} \approx K_2\, N\, a \tag{1.14}$$

K_2 being the uniaxial anisotropy. The equilibrium wall thickness results from the minimization of the sum

$$\sigma_{ex} + \sigma_{an} \approx J\, S^2\, \frac{\pi^2}{N\, a^2} + K_2\, N\, a \tag{1.15}$$

with respect to N.

In Fig. 1.8 the dependence of the total energy density $b/N + cN$ (b and c are the abbreviations of the prefactors of N) on N for a bulk-like Fe/Cu(100) film is depicted. The minimum of the energy density yields the equilibrium number of spins $N_0 = \sqrt{b/c} = \sqrt{J\, S^2\, \pi^2 / K_2^{\text{eff}}\, a^3} = 147$, which contribute to the rotation within the domain wall of the width $w = N_0\, a \approx \pi\sqrt{A/K_2^{\text{eff}}}$. The according surface energy density is given by $\sigma_{dw} \approx 2\pi\sqrt{A\, K_2^{\text{eff}}}$, where $A = J\, S^2/a = 1 \times 10^{-11}$ J/m is the exchange stiffness constant. The parameters[5] used to determine N_0 are $J = 2.16 \times 10^{-21}$ J, $K_2^{\text{eff}} = 4.2 \times 10^4$ J/m^3, $S = 1$ and $a = 2.86 \times 10^{-10}$ m (values taken from Ref. [16], p.408 and 413). The wall width corresponding to $N_0 = 147$ is about 42 nm. Since domain walls form a *continuous* transition between two domains, there is no unique definition of the domain width. The classical definition is based on the slope of the magnetization angle, and it is consistent with the wall width determined by the minimization of the total energy density. However, for domain imaging methods using electrons, which detect the projection of the magnetization within a domain wall, the width of a 180°-wall is given by $w = 2\sqrt{A/K_2^{\text{eff}}}$ (p. 219 of Ref. [17]).

Fig. 1.9 illustrates the rotation of the magnetization vector from one domain to the other through the two simplest cases of a 180°-domain wall, i. e. a Bloch wall (a) and a Néel wall

[5] The value of the exchange integral is determined from $J = 0.15\, k_B\, T_C$ [16] using $T_C = 1043$ K for bulk bcc Fe

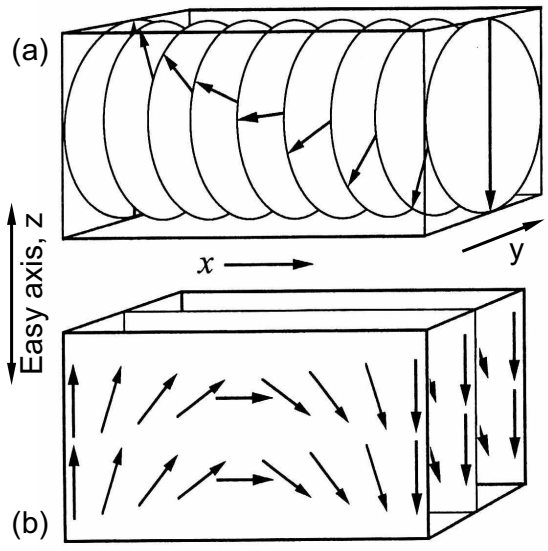

Figure 1.9: Rotation of the magnetization between two domains of a uniaxial material through a 180°-wall. Two different rotation modes are shown: The Bloch wall (a) is the optimum mode, whereas the Néll wall (b) is less favorable here but can be preferred in ultrathin films and in applied fields. The opposite reorientation direction is possible for both modes. (From [17]).

(b). The magnetic moments in a Bloch wall rotate in the y-z-plane, whereas the x-z-plane is the plane of rotation in a Néel wall with z being the easy axis of the magnetization. If the thickness of a thin film with an in-plane anisotropy becomes comparable to the Bloch wall width, a transition between two domains via an in-plane rotation like in Néel walls has a lower energy than a Bloch wall. Fig. 1.10 shows the model for a Bloch and a Néel wall approximated by an elliptical cylinder of width W and height D. The demagnetizing factor of this cylinder along the perpendicular magnetization direction is $N_{\text{Bloch}} = W/(W + D)$ for a Bloch wall and $N_{\text{Neel}} = D/(W + D)$ for a Néel wall, which is smaller than N_{Bloch} for $W > D$. A transition between the two wall modes, which is connected with a minimum in wall width and a maximum in the specific wall energy, was predicted by Néel [17]. The right hand side of Fig. 1.10 illustrates that the reduction of the magnetic charges due to an in-plane oriented external magnetic field, applied perpendicular to the easy axis of the magnetization, is much more pronounced in Néel walls as compared to Bloch walls. In complex composite walls, termed cross-tie walls [98], the energy is even lower than in a 180°-Néel wall because they consist mainly of energetically favorable 90°-walls. However, this kind of walls generally do not occur in ultrathin films. In the center of ultrathin films with perpendicular anisotropy domain walls are generally considered to be Bloch walls. At the surface the stray field of the domains acts on the wall, which may result in a rotation of the surface near magnetic moments into the Néel wall mode, in order to avoid energetically unfavorable stray fields reaching into the vacuum.

Whereas domain walls in bulk materials generally scale with the exchange length of the anisotropy energy $\xi = \sqrt{A/K_2}$, walls in thin films scale with the exchange length of the stray field $\xi_d = \sqrt{A/K_d}$, which becomes important in Néel walls. A completely analytic

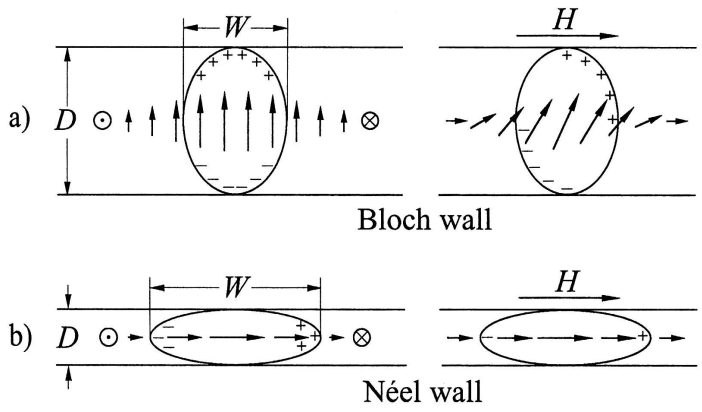

Figure 1.10: Cross section through a Bloch and a Néel wall in thin films of different thickness D and wall width W. The magnetic charges are indicated with and without applied field. (From [17]).

computation like for walls in the bulk is not possible in ultrathin films, where the wall profile needs to be explored by variational procedures or numerical test functions [17]. In particular, the problem of computing symmetric Néel walls is due to the decomposition of these walls into three parts of different scale: a sharply localized core interacts with two widely spread tails, in which a large part of the total rotation takes place. Riedel and Seeger [99] found an approach to solve this issue by separating the mathematical description into a differential equation for the core and an integral equation for the tail. The analytic solution for the core yields:

$$W_{core} \;=\; 2\sqrt{A(1-h^2)/[(K_2+K_d)(1-c_0)^2]} \tag{1.16}$$

where c_0 is the so-called core-tail boundary value which can range from $h = \frac{H\,M_s}{2\,K_2}$ to 1, H being an in-plane magnetic field perpendicular to the easy axis, and M_S is the saturation magnetization. The tail width, which is determined by the balance of the stray field energy (K_d) and the anisotropy energy density (K_2), reads:

$$W_{tail} \;=\; e^{-\gamma}\,D\,K_d/K_2 \tag{1.17}$$

where $\gamma \approx 0.577$ is Euler´s constant and D is the film thickness. The opposite effect of the stray field energy on the core width and the tail width is apparent: As K_d increases, the core width decreases while the tail width increases.

A consequence of the extended tails of a Néel wall is the interaction between them in an ultrathin film. Depending on the direction of rotation, i. e. the chirality, Néel walls can attract each other in the case of opposite chirality, ‘because they generate opposite charges in their overlapping tails’ [17]. If they are not pinned they can annihilate each other or can form double walls as observed for a Mo-Permalloy film of 14.7 nm thickness [15,100]. In the case of equal chirality the walls repel each other, which results in large in-plane magnetized domains. Again, domain wall pinning at defect sites or substrate step edges can limit the domain size. The interaction of Néel walls was found to extent over distances on the order of 100 μm in 50 nm thick Permalloy films [17].

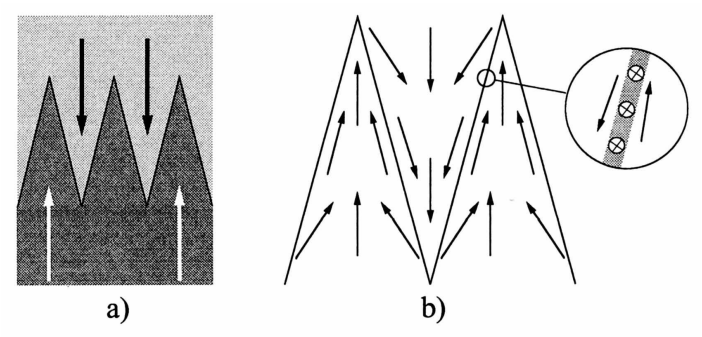

Figure 1.11: Zigzag-shaped charged domain wall separating two domains meeting "head-on" (a) and the formation of an uncharged Bloch type core within a zigzag wall. (From [17]).

Contrary to bulk materials, charged walls can be frequently observed in thin films. One typical situation of a charged wall is depicted in Fig. 1.11 (a) where two domains meet "head-on". In this situation the separating domain wall develops a sawtooth shape to reduce the charge density, which would be highest for a straight wall. As the zigzag angle is decreased the charge density is decreased at the expense of wall surface. In order to reduce the stray field energy in the vicinity of the core, long-range tails are formed comparable to the tails of Néel walls. The core remains almost uncharged at an alignment of the magnetization as shown in Fig. 1.11 (b). This concept was introduced by Finzi and Hartmann [101], and it was experimentally confirmed for materials used as magnetic storage media [102–104]. Depending on the film thickness, the core which is sketched to be of Bloch type in Fig. 1.11 (b) can also be that of a Néel or cross-tie wall [17].

Considering the size Δ of perpendicularly magnetized domains as a function of the layer thickness d, the theory of Kittel [18] predicts an increase of the domains according to $\Delta \propto \sqrt{d}$. However, experimentally a linear increase of the domain size with increasing thickness was found for ultrathin Co/Au(111) films below the thickness of the spin-reorientation transition [105]. This linear increase as a function of the thickness can be understood, if the thickness dependent surface anisotropy part $2K_2^S/d$ makes the major contribution to the effective anisotropy, i. e. for ultrathin films. If the volume contribution K_2^V is neglected, the domain width Δ may be written as $\Delta = \sqrt{\sigma/2K_2^S}\, d$, σ being the energy density per unit area of a 180°-domain wall between two domains [106]. In in-plane magnetized ultrathin layers, where the stray field lies in the film, the size of the domains can be orders of magnitude larger. This can be understood in terms of a repulsive interaction of Néel walls, which are energetically favorable in ultrathin in-plane magnetized films [17].

1.3.3 The stripe domain state

At the onset of ferromagnetic order as a function of the thickness in an ultrathin film with perpendicular anisotropy, as well as in the vicinity of the spin-reorientation transition or magnetization reversal at the SRT by an in-plane oriented external field (e. g. [107]), a perpendicular single

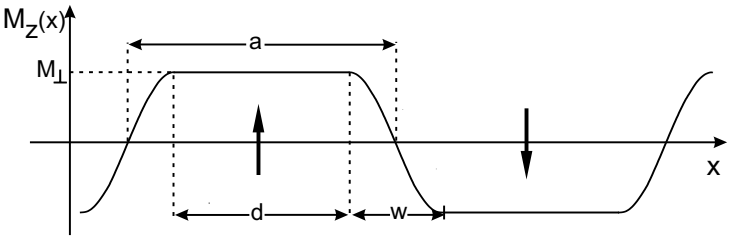

Figure 1.12: Profile of a perpendicularly magnetized stripe domain state of a monolayer. $M_z(x)$ varies as $\cos(\pi x/w)$. The arrows indicate the orientation of the magnetization. After [108].

domain state is unstable. This is due to the fact that the surface contribution of the magnetocrystalline anisotropy $2K_2^S > 0$ becomes weaker compared to the long-range dipolar interaction, which favors an in-plane orientation of the magnetization. At a still sufficiently large $2K_2^S$ the magnetization does not reorient into the plane, but the domains break up into alternating up and down magnetized stripe domains, whereby the stray field energy is reduced. The reduction of the stray field energy, however, is accompanied by an increase of domain wall energy, leading to a spatially modulated magnetic structure near the spin-reorientation transition, which in the simplest case is a stripe pattern.

Yafet and Gyorgy [108] calculated the profile of a stripe domain pattern of a monolayer with perpendicular anisotropy at $T = 0$. They assumed a simple domain configuration of a film lying in the x-y-plane as illustrated in Fig. 1.12. The profile of the magnetization varies along the x-axis with the period $2a$ and is constant in y-direction. The stripes are separated by domain walls, in which the magnetization rotates in the y-z-plane according to a Bloch wall which has a lower energy than a Néel wall for perpendicularly magnetized films. In the regions of the width $d = a - w$ the perpendicular component of the magnetization is constant and equals the saturation magnetization M_0:

$$M_z(x) \;=\; \pm M_0 \tag{1.18}$$

In the regions w the z- and the y-component of the magnetization are given by:

$$M_z(x) \;=\; \pm M_0 \,\cos\!\left(\frac{\pi x}{w}\right) \tag{1.19}$$

$$M_y(x) \;=\; \pm\sqrt{M_0^2 - M_z^2}. \tag{1.20}$$

Minimization of the total energy, which is the sum of the dipolar stray field energy, the anisotropy energy and the exchange energy, with respect to $\delta = \frac{w}{a}$ leads to the energetic description of the domain pattern of a ferromagnetic monolayer. The domain configuration turns out to be very sensitive to the dimensionless quantity

$$f \;=\; \frac{K_2^S}{\frac{1}{2}\mu_0 M_0^2\; a_0\; c} \tag{1.21}$$

in which K_2^S is the positive surface anisotropy, $c = 1.0782$ is specific to the square lattice and reflects its discreteness, and a_0 is the lattice constant. The minimum value $f = f_{\min}$, for which

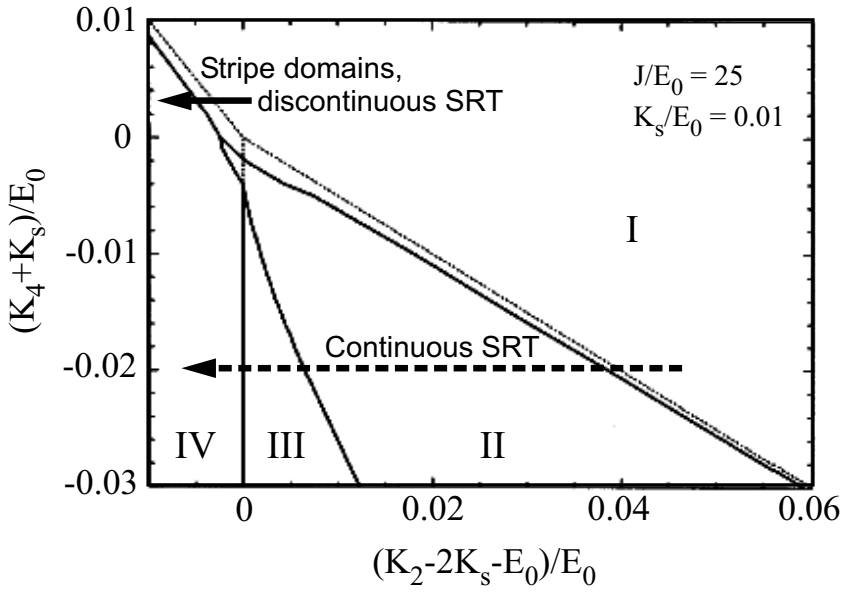

Figure 1.13: Magnetic phase diagram of a monolayer at $T = 0$ in the (K_2, K_4) plane. Assuming a periodic domain structure four different magnetic phases are separated by the solid lines: a domain phase with a perpendicular (I) and a canted (II) orientation of the magnetization within the domains, and uniform phases with a canted (III) and an in-plane (IV) magnetization. The dotted lines indicate the boundaries between magnetic phases if only uniform phases are considered. From [11].

domains occur corresponds to $\delta = 1$ and, as f increases from f_{min}, the domain configuration becomes energetically stable. Moreover, at $\delta = \frac{w}{a} = 1$ the profile of the domain pattern is purely cosine-like, i. e. the flat part d in Fig. 1.12 has shrunk to zero. This occurs as a consequence of the strong exchange energy competing only with the weak dipolar energy. An increase of f of only 4% corresponds to a reduction of δ by two orders of magnitude and results in a drastic increase of the domain size. Typical values for which domains are stable are given by $1 < f < 1.4$.

Jensen *et al.* [11] calculated the magnetic phase diagram of a monolayer at $T = 0$ in the $(K_2 - K_4)$ plane as shown in Fig. 1.13. By taking second- and fourth-order uniaxial anisotropies into account, they point out the role of the domain formation, using ratios of the exchange coupling J, the demagnetizing energy E_0 and the quartic in-plane anisotropy of the (100) face K_s of $J/E_0 = 25$ and $K_s/E_0 = 0.01$ appropriate for $3d$ transition metals. In agreement with Ref. [108] 'for $K_4 = K_s = 0$, a stripe domain phase with a perpendicular orientation of the domains is more favorable than the uniform perpendicular magnetization for large values of $K_2 > E_0$' [11] (region I). Within this phase, for $(K_4 + K_s)/E_0 > 0$, the width of the stripe domains decreases almost exponentially with decreasing K_2 until a cosine-like profile of the stripe domain pattern is reached and a discontinuous SRT to the uniform in-plane magnetization (region IV) occurs. This is indicated by the solid arrow in Fig. 1.13. In contrast, for $(K_4 +$

$K_s)/E_0 < 0$, the domain width does not decrease any longer with decreasing K_2, but it stays almost constant within the canted domain phase (region II), while the canting angle of the magnetization rises. The domain width increases again at the value of K_2, where the canted uniform magnetization emerges (region III), and the canting angle further rises until finally, an in-plane magnetized single domain state occurs for $(K_2 - 2K_s - E_0)/E_0 < 0$ (region IV) [11,109]. This continuous SRT is indicated by the dotted arrow in Fig. 1.13. For comparison, the dotted lines in the figure indicate the boundaries between magnetic phases if only uniform phases are considered.